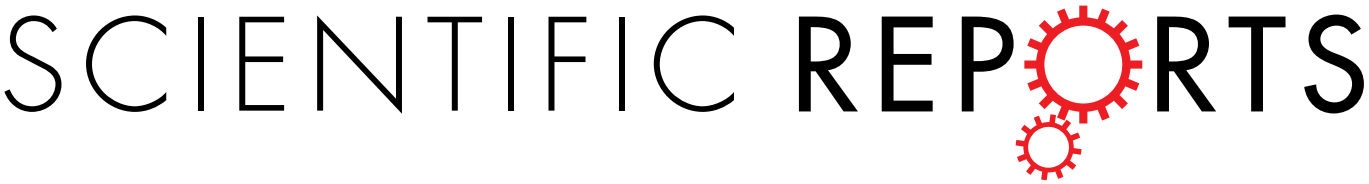

OPEN

Epitaxial stabilization and phase instability of VO_2 polymorphs

Shinbuhm Lee, Ilia N. Ivanov, Jong K. Keum & Ho Nyung Lee

Received: 10 August 2015
Accepted: 25 November 2015
Published: 20 January 2016

The VO_2 polymorphs, i.e., VO_2(A), VO_2(B), VO_2(M1) and VO_2(R), have a wide spectrum of functionalities useful for many potential applications in information and energy technologies. However, synthesis of phase pure materials, especially in thin film forms, has been a challenging task due to the fact that the VO_2 polymorphs are closely related to each other in a thermodynamic framework. Here, we report epitaxial stabilization of the VO_2 polymorphs to synthesize high quality single crystalline thin films and study the phase stability of these metastable materials. We selectively deposit all the phases on various perovskite substrates with different crystallographic orientations. By investigating the phase instability, phonon modes and transport behaviours, not only do we find distinctively contrasting physical properties of the VO_2 polymorphs, but that the polymorphs can be on the verge of phase transitions when heated as low as ~400 °C. Our successful epitaxy of both VO_2(A) and VO_2(B) phases, which are rarely studied due to the lack of phase pure materials, will open the door to the fundamental studies of VO_2 polymorphs for potential applications in advanced electronic and energy devices.

Vanadium dioxides (VO_2) are strongly correlated d^1 electron systems and are known to have several polymorphs, which include VO_2(A), VO_2(B), VO_2(M1) and VO_2(R). While the chemical formula is the same, their crystalline and electronic structures are completely different and highly complex, exhibiting many interesting electrical, optical and chemical properties owing to the strong electron correlation[1–3]. Among the aforementioned VO_2 polymorphs, the rutile VO_2(R) and the monoclinic VO_2(M1) have been the most widely studied phases due primarily to their metal-to-insulator transition (MIT) temperature close to room temperature (68 °C)[1–3]. Since this phase transition is accompanied by a huge change in resistivity by three orders of magnitude, VO_2(R) and VO_2(M1) have attracted tremendous attention for the electronic and optical applications, such as smart windows[4], frequency-agile metamaterials[5,6] and electrical switches[7–9].

The monoclinic VO_2(B) phase has also been explored. However, the focus has been on utilization of the open framework, which originates from the edge-sharing VO_6 octahedra[10–12]. Such open framework makes VO_2(B) a promising energy material, which can be used as electrodes in Li-ion batteries[13]. Chen *et al.* first reported the growth of textured VO_2(B) films on (001)-oriented $SrTiO_3$ substrates[14], but pure phase could be stabilized only at thin (<25 nm) films. It is known that the growth of single crystalline VO_2(B) is very challenging due to the complex crystal structure[14,15]. Similarly, the study of the tetragonal VO_2(A) has so far been very limited[15–17] as compared to other VO_2 polymorphs, due to the difficulty in synthesizing phase pure crystals. Thus, their physical properties and potential for technical applications have not been much explored.

One of the main reasons for the difficulty in preparing phase pure VO_2 polymorphs is the narrow range of phase diagram[3] and, more importantly, the VO_2 polymorphs are closely related to each other in a thermodynamic framework[10,12,16]. For example, it has been shown that the VO_2(A) and VO_2(B) phases are metastable in bulk and undergo an irreversible phase change into VO_2(R) upon heating[10,12,16], resulting in a mixture of VO_2 polymorphs. The formation of such mixed phases hinders the accurate understanding of the physical properties of the VO_2 polymorphs. Hence, preparation of phase pure and high quality crystalline materials has been one of the major challenges in VO_2 research.

Epitaxial stabilization of crystalline materials by formation of low energy interface is a well-known approach to creating pure phase materials[18–22]. Because the stability of these non-equilibrium materials is affected by both thermodynamic and kinetic factors, the highly non-equilibrium film growth conditions offered by pulsed laser epitaxy (PLE) provide a unique opportunity to discover a wide range of materials with unprecedented functionalities.

Here, we report comparatively the physical properties of four VO_2 polymorphs (i.e., R, M1, A and B phases) epitaxially stabilized by PLE on various perovskite substrates with different crystallographic orientations, i.e.,

Oak Ridge National Laboratory, Oak Ridge, Tennessee 37831, USA. Correspondence and requests for materials should be addressed to H.N.L. (email: hnlee@ornl.gov)

VO_2 polymorphs	Crystal structure (space group)	Lattice constants in bulk				Substrates for epitaxial growth	Critical growth condition
		a (Å)	*b* (Å)	*c* (Å)	β (°)		
VO_2(A)	Tetragonal ($P4_2/ncm$ (138))	8.43	8.43	7.68		STO(011), LAO(011)	$T_s < 430$ °C
VO_2(B)	Monoclinic (C2/m (12))	12.03	3.69	6.42	106.6	pc-TSO(001), STO(001), LSAT(001), LAO(001), pc-YAO(001)	$T_s < 430$ °C
VO_2(M1)	Monoclinic ($P2_1/c$ (14))	5.38	4.52	5.74	122.6	STO(111), LSAT(111), LAO(111)	Not critical to T_s
VO_2(R)	Tetragonal ($P4_2/mnm$ (136))	4.55	4.55	2.86		Thermal heating of VO_2(M1) above 68 °C	

Table 1. Crystal structure, lattice parameters and growth conditions for VO_2 polymorphs.

ABO_3(001), ABO_3(011) and ABO_3(111). Distinctively contrasting phase stability, lattice motions and transport properties reported here will provide useful information to develop VO_2-based electronic devices and energy materials.

Results and Discussion

In order to selectively grow VO_2 polymorphs, commercially-available perovskite-oxide substrates, including $TbScO_3$ (TSO), $SrTiO_3$ (STO), $(LaAlO_3)_{0.3}(SrAl_{0.5}Ta_{0.5}O_3)_{0.7}$ (LSAT), $LaAlO_3$ (LAO) and $YAlO_3$ (YAO), were used. As summarized in Table 1, we were able to epitaxially grow (1) the tetragonal VO_2(A) phase on (011)-oriented STO and LAO substrates; (2) the monoclinic VO_2(B) phase on a wide selection of (001)-oriented substrates, including pseudo-cubic TSO, STO, LSAT, LAO and pseudo-cubic YAO; and (3) the monoclinic VO_2(M1) phase on (111)-oriented STO, LSAT and LAO substrates, which commonly have a 3*m* surface symmetry.

The selective growth occurs due to preferential in-plane lattice matching of perovskite-oxide substrates with the VO_2 polymorphs. VO_2(B) has a low-symmetry monoclinic structure (space group of C2/m (12)) with lattice constants of $a = 12.03$ Å, $b = 3.69$ Å, $c = 6.42$ Å and $\beta = 106.6$°, as summarized in Table 1 and as schematically shown in Fig. 1a. Various X-ray diffraction (XRD) scans, including $\theta-2\theta$ scans shown in Fig. 2a and ϕ scans shown in Fig. 2d, for VO_2(B) films on (001)STO ($a_{STO} = 3.905$ Å) confirmed the following epitaxy relationship: (001)VO_2(B) || (001)STO and [100]VO_2(B) || [100]STO (see Fig. 2g). The lattice mismatch $(a_{sub} - a_{film})/a_{sub} \times 100$ was -2.6% for [010]VO_2(B) || [010]STO and $+5.8$% for [100]VO_2(B) || [100]STO, where the negative and positive signs indicate compressive and tensile strain, respectively.

VO_2(A) has a tetragonal structure (space group of $P4_2/ncm$ (138)) with lattice constants of $a = b = 8.43$ Å and $c = 7.68$ Å, as schematically shown in Fig. 1b. We found that the single crystalline VO_2(A) phase could be grown best on (011)STO with the following epitaxy relationship: (100)VO_2(A) || (011)STO and [010]VO_2(A) || [011]STO (see Fig. 2h), as confirmed by XRD $\theta-2\theta$ scans (see Fig. 2b) and ϕ scans (see Fig. 2e). The mismatches along the two orthogonal directions, i.e., [010]VO_2(A) || [011]STO and [001]VO_2(A) || [100]STO are -1.7 and $+1.7$%, respectively.

The VO_2(M1) phase has a low-symmetry monoclinic structure (space group of $P2_1/c$ (14)) with lattice constant of $a = 5.38$ Å, $b = 4.52$ Å, $c = 5.74$ Å and $\beta = 122.6$°, as schematically shown in Fig. 1c. There have been several reports on the successful growth of VO_2(M1) films on substrates with a 3*m* surface symmetry[23] such as (0001)Al_2O_3, (111)$MgAl_2O_4$, (111)MgO and (0001)ZnO. In our study, we mainly attempted to grow epitaxial films on (111)STO substrates to unify the substrates for VO_2 polymorph films. Since the XRD peak positions of VO_2(M1) are very close to those of the STO substrate, the film peaks are hardly observed in Fig. 2c. Nevertheless, as confirmed by XRD ϕ scans (see Fig. 2f), VO_2(M1) could be grown on (111)STO with the following epitaxy relationship: (010)VO_2(M1) || (111)STO and [001]VO_2(M1) || [$\bar{2}$11]STO, as illustrated in Fig. 2i (see the left portion). The lattice mismatch is -3.8% along the [001]VO_2(M1) || [$\bar{2}$11]STO and $+2.6$% along the [100]VO_2(M1) || [1$\bar{2}$1]STO.

While the three VO_2 phases listed above are accessible at room temperature from as grown films, we also tried to access to the VO_2(R) phase via a structural phase transition by heating a VO_2(M1) film above the T_c (68 °C). The VO_2(R) has a tetragonal structure (space group of $P4_2/mnm$ (136)) with lattice constants of $a = b = 4.55$ Å and $c = 2.86$ Å, as schematically shown in Fig. 1d. As shown in the inset of Fig. 2c, we were able to confirm the phase transition into the VO_2(R) phase by performing an XRD $\theta-2\theta$ scans at 100 °C, which is higher than the T_c. Both VO_2(R) and VO_2(M1) phases on (111)STO are (010)-oriented. The epitaxial relationship for VO_2(R) on (111)STO is illustrated in Fig. 2i (see the right portion) as follows: (010)VO_2(R) || (111)STO and [100]VO_2(R) || [$\bar{2}$11]STO with the lattice mismatch of $+4.9$% along the [100]VO_2(R) || [$\bar{2}$11]STO direction and -3.6% along the [001]VO_2(R) || [01$\bar{1}$]STO direction.

Among the growth parameters, we found that a proper choice of the substrate temperature, T_s, is critical, in particular for VO_2(A) and VO_2(B) phases on perovskite substrates. As shown in Table 1, we could reproducibly grow VO_2(A) and VO_2(B) phases when T_s was lower than 430 °C. On the other hand, the growth of VO_2(M1) phase was quite insensitive to T_s as we confirmed the growth of high quality films in a wide temperature window ($400 \leq T_s \leq 600$ °C).

To evaluate the thermal stability of VO_2 polymorphs, epitaxial films of VO_2(A), VO_2(B) and VO_2(M1) phases were heated up to 600 °C. We kept the samples in vacuum (~0.37 Torr) to avoid spontaneous oxidation into the V_2O_5 phase[24]. Fig. 3a,b show the phase evolution of VO_2(B)/STO(001) and VO_2(A)/STO(011), respectively, characterized by XRD $\theta-2\theta$ scans as a function of temperature. In case of VO_2(B) on STO(001), upon heating, XRD peaks corresponding to (00*l*) VO_2(B) disappeared above 430 °C and then the (330) VO_2(A) peak subsequently appeared above 440 °C, indicating the formation of polycrystalline VO_2(A). When we further increased T_s, the VO_2(A) phase disappeared above 470 °C, and the polycrystalline VO_2(R) phase appeared above 520 °C. This transformation, i.e., VO_2(B) → VO_2(A) → VO_2(R), indicates that the structural frameworks are similar among the

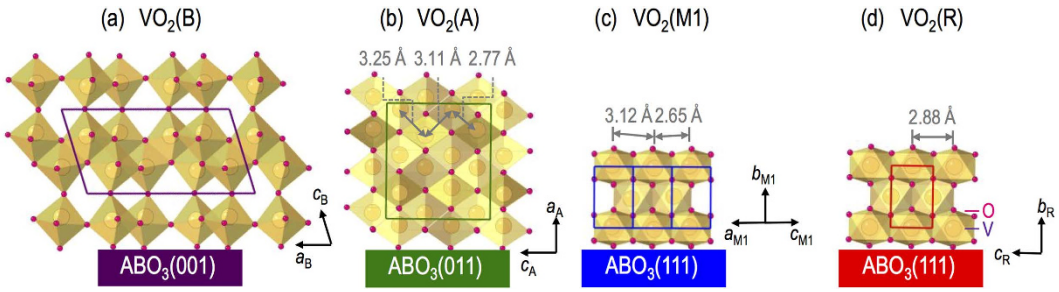

Figure 1. Schematics of (a) VO_2(B), (b) VO_2(A), (c) VO_2(M1) and (d) VO_2(R) phases grown on various perovskite substrates with different crystallographic orientations, i.e., ABO_3(001), ABO_3(011) and ABO_3(111), respectively.

phases. The first transition to A-phase is known to associate with the realignment of VO_6 octahedra from edge shared to face shared[10] and, the second transition to the R-phase is attributed to the reorientation of the half of the VO_6 octahedra[10].

As shown in Fig. 3b, the VO_2(A)/STO(011) also revealed similar thermal stability. The peaks corresponding to (l00) VO_2(A) disappeared above 430 °C and polycrystalline VO_2(R) was subsequently formed above 470 °C. The phase transitions of both VO_2(B) and VO_2(A) were irreversible upon cooling. The irreversible phase transformation of VO_2 polymorphs is similar to what was observed in other binary oxide polymorphs. For example, TiO_2 is known to undergo a transition from the anatase to the rutile phase via brookite[25]. As the crossover instability in TiO_2 polymorphs was understood by closely balanced enthalpy among these phases[26], further thermodynamic studies will be useful to understand the phase instability in VO_2. The thermal instability of VO_2(A) and VO_2(B) explains the formation of mixed phase VO_2 polymorphs with VO_2(R) as an impurity phase often observed from films grown above 430 °C. The observation of MIT at 68 °C in VO_2(A) and VO_2(B) films grown above 430 °C clearly indicates inclusion of VO_2(R) as an impurity phase[14]. We note that, on the other hand, the VO_2(M1) phase was converted into VO_2(R) at ~68 °C upon heating and was stable up to 600 °C (data not shown). Upon cooling, VO_2(R) was converted back to VO_2(M1), indicating a reversible phase evolution with good thermal stability.

Since the VO_2 polymorphs have distinct structures, one can expect highly contrasting vibrational characteristics of lattice. Thus, identifying the phonon mode is a good measure of phase purity. In order to comparatively understand the phonon modes, Raman spectroscopy was carried out for the VO_2 polymorphs by growing films on LAO substrates. The latter were used because dominant Raman spectral features of LAO are isolated at very low wavelength (32 and 123 cm^{-1})[27]. As shown in Fig. 4, the VO_2 polymorphs revealed contrasting Raman spectra compared to each another. As compared to Raman data available from nanostructured materials[28–30], we were able to confirm the phase purity of our epitaxial films.

In addition to the phase confirmation, the Raman spectra from VO_2 provide more detailed information about the local structure. There are three sets of V−O modes[31] within wavenumber of 100−1100 cm^{-1}. At low wavenumber (<400 cm^{-1}), the bands are assigned to V−O−V bending modes; at intermediate wavenumber (400−800 cm^{-1}), the bands are attributed to V−O−V stretching modes; and at high wavenumber (>800 cm^{-1}), the bands are assigned to V=O stretching modes of distorted octahedra and distorted square-pyramids. As shown in Fig. 4a, the phonon modes in epitaxial films of VO_2(B) were mainly observed at low and intermediate wavenumbers (152, 263 and 480 cm^{-1}), indicating that bending and stretching modes of V−O−V are dominant in VO_2(B). On the other hand, as shown in Fig. 4b, the phonon modes in VO_2(A) were mainly observed at high and intermediate wavenumbers (152, 485 and 887 cm^{-1}), which imply that the stretching modes of V−O−V and V=O are dominant lattice motions in VO_2(A). The phonon modes in VO_2(M1) are very complex and composed of stretching and bending of V−O−V and zigzag chains of V−V. The phonon modes in VO_2(R) dominantly include stretching modes of V−O−V, which indicate that the crystal structure of VO_2(R) is more symmetric than VO_2(M1)[30,32,33].

While the transport properties of VO_2(M1) and VO_2(R) have been extensively studied[1–3,8,9,24,32–34], the physical properties of VO_2(B) and VO_2(A) phases have not been much explored due to difficulty in preparing phase pure thin films. Figure 5 shows the transport characteristics of VO_2(B), VO_2(A) and VO_2(M1) films grown on STO substrates. VO_2(A) showed a monotonic decrease of resistivity as increasing the temperature, typical for insulators. While still insulating over the temperature range we measured, VO_2(B) revealed more or less semiconducting behaviours with much smaller resistivity compared to that of VO_2(A), i.e., $\rho^{300\,K}_{VO_2(B)} \approx 0.02\ \Omega \cdot$ cm and $\rho^{300\,K}_{VO_2(A)} \approx 60\ \Omega \cdot$ cm. The resistivity in our VO_2(A)/STO(011) is higher than that reported in VO_2(A)/STO(001)[15] by one order of magnitude. The reason is unclear, but one can consider that the film on (001)STO is under a different strain state or that the growth on a (001)STO substrate may include a small amount of VO_2(B) since their thermal phase boundary is relatively low[10,12,16], as shown in Fig. 3. In the case of VO_2(M1) phase, we also observed the MIT at 340 K from VO_2(M1) to VO_2(R) phase change upon heating, similarly observed from many previous studies[1–3,8,9,24,32–34]. The MIT accompanied a sudden decrease of the resistivity by 3−4 orders of magnitude, which is comparable to high quality epitaxial films grown on Al_2O_3(0001)[24]. This excellent performance could be attributed to the high crystallinity of our epitaxial films ($\Delta\omega < 0.1^o$). The transition temperature is consistent with structural phase transition from VO_2(M1) to VO_2(R), as shown in XRD $\theta-2\theta$ scan in the inset of Fig. 2c. We note

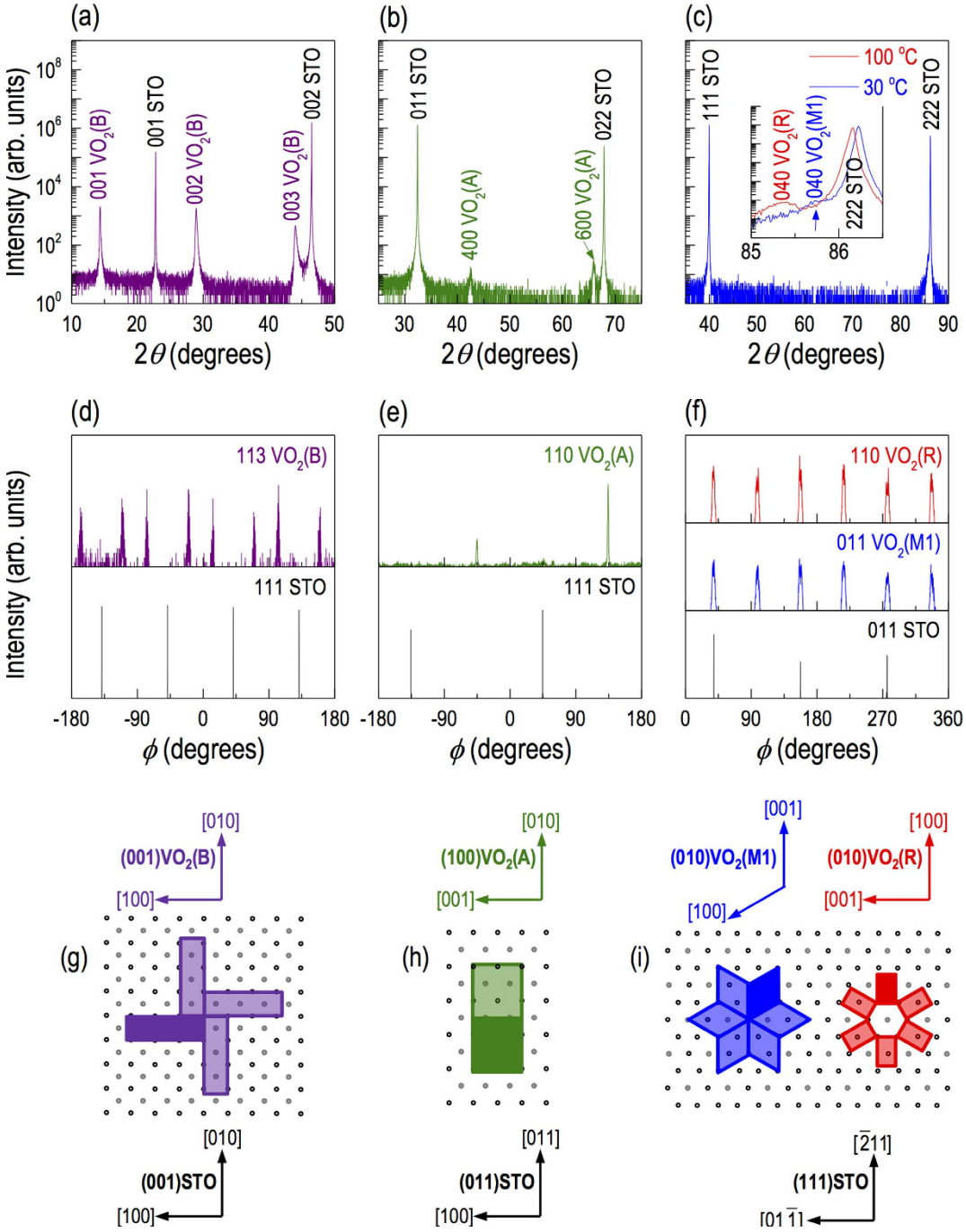

Figure 2. XRD $\theta-2\theta$ scans of (a) VO_2(B), (b) VO_2(A) and (c) VO_2(M1) thin films on STO (001), (011) and (111) substrates, respectively. The inset in (c) shows XRD scans of the VO_2(R) phase (red line) obtained at 100 °C by heating the VO_2(M1) film (blue line), which is above the $T_c = 68$ °C. From ϕ scans shown in (d) VO_2(B), (e) VO_2(A) and (f) VO_2(M1) and VO_2(R) thin films, in-plane lattice matching is schematically illustrated as shown in (g–i).

that the transport properties of the films grown on LAO substrates were almost identical except for slightly decreased resistivity for films on LAO (data not shown).

Overall, as explained above, the VO_2 polymorphs revealed a wide range of electronic ground states, i.e., metal [VO_2(R)], semiconductor [VO_2(B)] and insulator [VO_2(A) and VO_2(M1)], depending on their crystal structure. This wide range of electronic ground states makes VO_2 highly attractive over other transition metal dioxides, since most other binary oxides are either metal (CrO_2: α-phase and β-phase) or insulator (TiO_2: rutile, brookite and anatase). While it is not the main focus of this paper, it is worth mentioning that Goodenough[32,34] obtained a

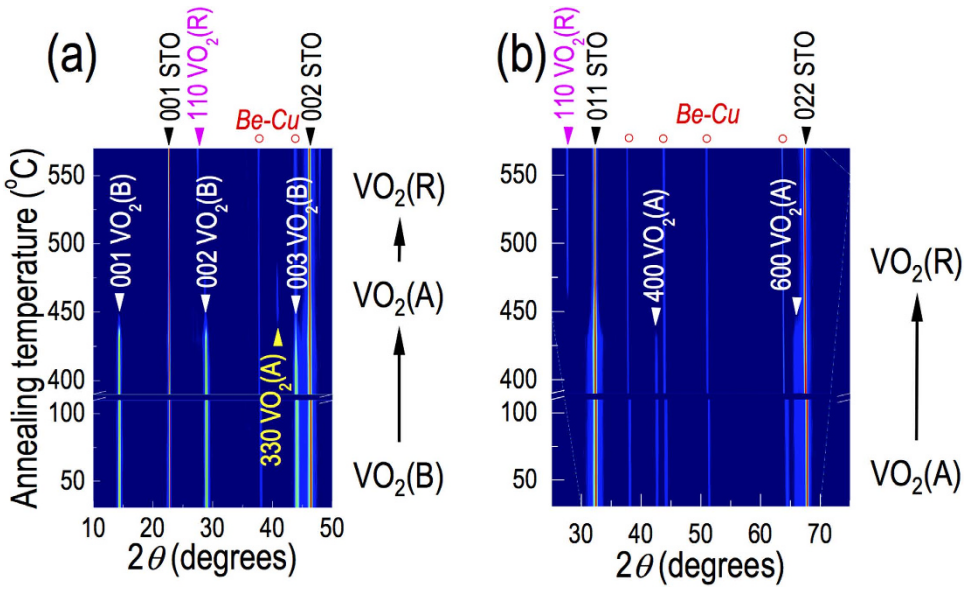

Figure 3. Real time XRD $\theta-2\theta$ scans of (a) VO_2(B)/STO(001) and (b) VO_2(A)/STO(011) samples as a function of temperature in 0.37 Torr of air. A clear phase change was observed from both samples, indicating that the phases are in close proximity with each other. The phase changes were, however, irreversible upon cooling. It is also worth noting that there are temperature gaps where the XRD peaks are hardly seen before showing up the polycrystalline phases. They are 470–520 °C in (a) and 430–470 °C in (b). We attribute this to the films in metastable state undergoing polycrystallization during the phase transition, even though it is hard to clearly identify due to the suppressed XRD peaks.

semiempirical expression for the room temperature critical V−V separation $R_c \approx 2.92-2.94$ Å for localized and itinerant 3*d* electrons in vanadium oxides.

$$R < R_c \rightarrow \text{Itinerant } 3d \text{ electron} \rightarrow \text{Metal};$$
$$R > R_c \rightarrow \text{Localized } 3d \text{ electron} \rightarrow \text{Insulator}.$$

This semiempirical criterion indicates that VO_2 polymorphs can be either metal or insulator depending on the V−V separation in the distinguishable crystal structures. The VO_2(R) phase has a uniform V−V separation of $R = 2.88$ Å (ref. 32), resulting in a metallic ground state. As shown in Fig. 1c, the VO_2(M1) phase has zigzag V−V chains of $R = 2.65$ Å and 3.12 Å (ref. 32). The VO_2(A) phase also has zigzag V−V chains of $R = 3.25$ Å, 3.11 Å and 2.77 Å (ref. 17) as shown in Fig. 1b. The insulating behaviours that we have observed for those M1 and A-phases are attributed to the localized electrons in shorter V−V chains with $R = 2.65$ Å [VO_2(M1)] and 2.77 Å [VO_2(A)]. Thus, overall transport behaviours of our epitaxial thin films can be well explained by Goodenough's criterion[32,34]. Since VO_2 polymorphs have a wide range of physical properties and, in particular, VO_2(B) phase is on the verge of becoming a metal, our report on epitaxial synthesis of high quality thin films can open the door to the discovery of novel phenomena and physical properties by deliberate control of the order parameters by various means, including strain, dimensionality, confinement, etc., which can be accessible via epitaxial heterostructuring.

In conclusion, we grew epitaxial films of VO_2 polymorphs. For the growth of phase pure VO_2 polymorphs, a careful selection of the growth conditions was necessary especially for the temperature and oxygen pressure. Depending on the crystal orientation of substrates, we found that different phases of VO_2 could be selectively grown, i.e., VO_2(B)/ABO_3(001), VO_2(A)/ABO_3(011), VO_2(M1)/ABO_3(111), and VO_2(R)/ABO_3(111). Such phases revealed unique phonon modes due to the distinctly different crystal structures and physical properties in spite of the same chemical composition. Since the VO_2 polymorphs have a wide range of electronic ground states from metal [VO_2(R)] and semiconductor [VO_2(B)] to insulator [VO_2(A) and VO_2(M1)], our epitaxial thin films, which are known to be challenging to grow, will expedite our understanding of underlying physics and developing VO_2 polymorphs-based electronic devices utilizing the wide selection of the electronic properties from a single composition.

Methods

Epitaxial film growth. We deposited epitaxial films (100 nm in thickness) of VO_2 polymorphs on perovskite oxide substrates by pulsed laser epitaxy. We ablated a sintered VO_2 target, which contains mainly the M1 phase, by a KrF excimer laser (248 nm in wavelength) at a laser fluence of 1 Jcm^{-2} and at a laser repetition rate of 10 Hz. By growing thin films under a wide range of $P(O_2)$ and T_s (2 mTorr $< P(O_2) <$ 25 mTorr and 350 °C $< T_s <$ 600 °C), we found the optimal condition for VO_2(A), VO_2(B) and VO_2(M1), as described in Table 1. It should be noted that V_2O_3 was formed at $P(O_2) <$ 5 mTorr and V_2O_5 was formed for $P(O_2) >$ 25 mTorr, due to the multivalent nature of vanadium[24].

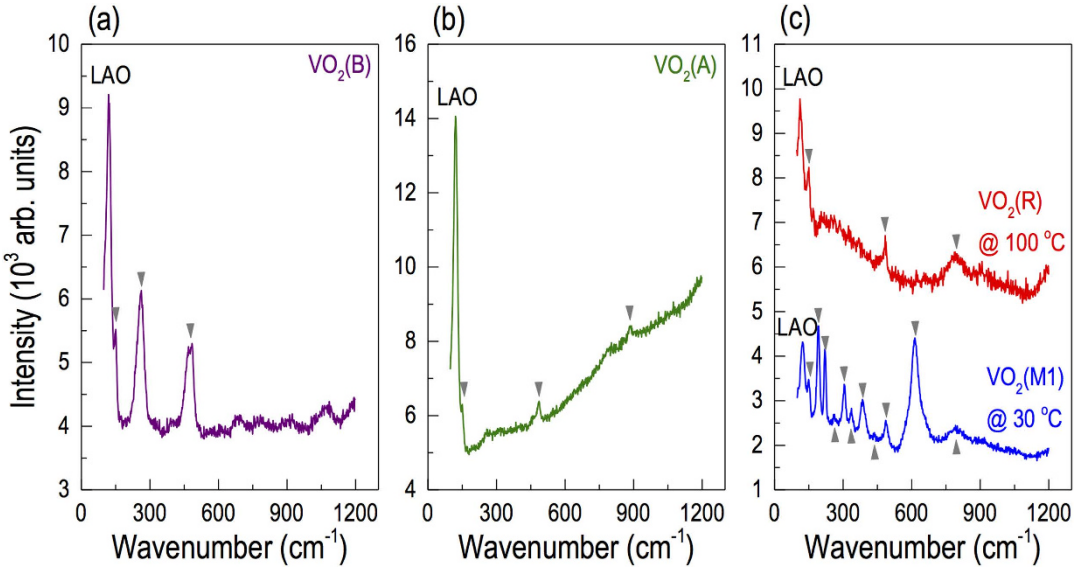

Figure 4. Raman spectra of (a) VO_2(B), (b) VO_2(A), (c) VO_2(M1) and VO_2(R) grown on LAO substrates. The spectra were recorded at room temperature except the VO_2(R) phase shown in (c), which was obtained by heating the M1 phase sample to 100 °C in air.

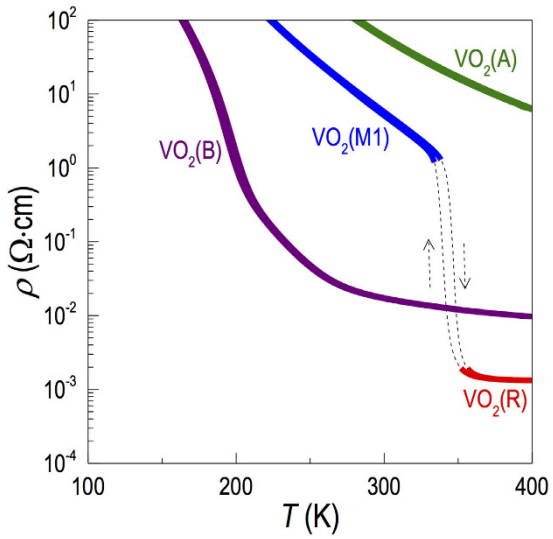

Figure 5. Temperature dependent resistivity for VO_2(B), VO_2(A), VO_2(M1) and VO_2(R) phases grown on (001), (011), and (111) STO substrates, respectively, exhibiting distinctly contrasting transport behaviours.

Characterization of physical properties. To investigate the *dc* transport properties, a physical property measurement system (Quantum Design Inc.) was used with Pt contacts in four-probe geometry. X-ray diffraction (XRD) measurements were carried out with a four-circle high-resolution X-ray diffractometer (X'Pert Pro, Panalytical) using the Cu-Kα_1 radiation equipped with a hot stage (DHS 900, Anton Paar). High-temperature environmental XRD measurements were conducted under vacuum with base pressure of 0.37 Torr air. Raman spectra were recorded at various temperatures using a temperature control stage (Lincam Scientific Instruments). A Renishaw 1000 confocal Raman microscope was used to measure Raman spectra in back scattering configuration. Each spectrum is a sum average of seven individual spectra taken at different place on the sample through 20× objective. The wavelength of the Raman laser used in these measurements was 532 nm.

References

1. Imada, M., Fujimori, A. & Tokura, Y. Metal-insulator transitions. *Rev. Mod. Phys.* **70,** 1039 (1998).
2. Basov, D. N., Averitt, R. D., Van der Marel, D., Dressel, M. & Haule, K. Electrodynamics of correlated electron materials. *Rev. Mod. Phys.* **83,** 471 (2011).

3. Yang, Z., Ko, C. & Ramanathan, S. Oxide electronics utilizing ultrafast metal-insulator transitions. *Annu. Rev. Mater. Res.* **41,** 337 (2011).
4. Zhou, J. *et al.* VO_2 thermochromic smart window for energy savings and generation. *Sci. Rep*. **3,** 3029 (2013).
5. Driscoll, T. *et al.* Mott transition in VO_2 revealed by infrared spectroscopy and nano-imaging. *Science* **325,** 1518 (2009).
6. Liu, M. *et al.* Terahertz-field-induced insulator-to-metal transition in vanadium dioxide metamaterial. *Nature* **487,** 345 (2012).
7. Chang, S. H. *et al.* Oxide double-layer nanocrossbar for ultrahigh-density bipolar resistive memory. *Adv. Mater.* **23,** 4063 (2011).
8. Nakano, M. *et al.* Collective bulk carrier delocalization driven by electrostatic surface charge accumulation. *Nature*, **487,** 459 (2012).
9. Jeong, J. *et al.* Suppression of metal-insulator transition in VO_2 by electric field-induced oxygen vacancy formation. *Science*, **339,** 1402 (2013).
10. Leroux, Ch., Nihoul, G. & Van Tendeloo, G. From VO_2(B) to VO_2(R): Theoretical structures of VO_2 polymorphs and *in situ* electron microscopy. *Phys. Rev. B* **57,** 5111 (1998).
11. Chernova, N. A., Roppolo, M., Dillon, A. C. & Whittingham, M. S. Layered vanadium and molybdenum oxides: batteries and electrochromics. *J. Mater. Chem.* **19,** 2526 (2009).
12. Zhang, S. *et al.* From VO_2(B) to VO_2(A) nanobelts: first hydrothermal transformation, spectroscopic study and first principles calculation. *Phys. Chem. Chem. Phys.* **13,** 15873 (2011).
13. Li, W., Dahn, J. R. & Wainwright, D. S. Rechargeable lithium batteries with aqueous electrolytes. *Science* **264,** 1115 (1994).
14. Chen, A. *et al.* Textured metastable VO_2(B) thin films on $SrTiO_3$ substrates with significantly enhanced conductivity. *Appl. Phys. Lett.* **104,** 071909 (2014).
15. Srivastava, A. *et al.* Selective growth of single phase VO_2(A, B and M) polymorph thin films. *APL Mater*. **3,** 026101 (2015).
16. Oka, Y., Sato, S., Yao, T. & Yamamoto, N. Crystal structures and transition mechanism of VO_2(A). *J. Solid State Chem.* **141,** 594 (1998).
17. Popuri, S. R. *et al.* VO_2(A): Reinvestigation of crystal structure, phase transition and crystal growth mechanisms. *J. Solid State Chem.* **213,** 79 (2014).
18. Lotnyk, A., Senz, S. & Hesse, D. Epitaxial growth of TiO_2 thin films on $SrTiO_3$, $LaAlO_3$ and yttria-stabilized zirconia substrates by electron beam evaporation. *Thin Solid Films* **515,** 3439 (2007).
19. Schlom, D. G., Chen, L.-Q., Pan, X., Schmeh, A. & Zurbuchen, M. A. Strain tuning of ferroelectric thin films. *J. Am. Ceram. Soc.* **91,** 2429 (2008).
20. Choi, W. S. *et al.* Atomic layer engineering of perovskite oxides for chemically sharp heterointerfaces. *Adv. Mater.* **24,** 6423 (2012).
21. Jeen, H. *et al.* Reversible redox reactions in an epitaxially stabilized $SrCoO_x$ oxygen sponge. *Nature Mater*. **12,** 1057 (2013).
22. Wenbin, W. *et al.* Room-temperature multiferroic hexagonal $LuFeO_3$ films. *Phys. Rev. Lett.* **110,** 237601 (2013).
23. Wong, F. J., Zhou, Y. & Ramanathan, S. Epitaxial variants of VO_2 thin films on complex oxide single crystal substrates with 3*m* surface symmetry. *J. Cryst. Growth* **364,** 74 (2013).
24. Lee, S., Meyer, T. L., Park, S., Egami, T. & Lee, H. N. Growth control of the oxidation state in vanadium oxide thin films. *Appl. Phys. Lett.* **105,** 223515 (2014).
25. Zhang, H. & Banfield, J. F. Understanding polymorphic phase transformation behavior during growth of nanocrystalline aggregates: insights from TiO_2. *J. Phys. Chem. B* **104,** 3481 (2000).
26. Ranade, M. R. *et al.* Energetics of nanocrystalline TiO_2. *PNAS* **99,** 6476 (2002).
27. Gasparov, L., Jegorel, T., Loetgering, L., Middey, S. & Chakhalian, J. Thin film substrates from the Raman spectroscopy point of view. *J. Raman Spectrosc.* **45,** 465 (2014).
28. Wu, X., Tao, Y., Dong, L., Wang, Z. & Hu, Z. Preparation of VO_2 nanowires and their electric characterization. *Mater. Res. Bull.* **40,** 315 (2005).
29. Hou, J., Zhang, J., Wang, Z., Zhang, Z. & Ding, Z. Structural transition of VO_2(A) nanorods studied by vibrational spectroscopies. *RSC Adv*. **4,** 18055 (2014).
30. Ji, Y. *et al.* Role of microstructures on the M1-M2 phase transition in epitaxial VO_2 thin films. *Sci. Rep.* **4,** 4854 (2014).
31. Hardcastle, F. D. & Wachs, I. E. Determination of vanadium−oxygen bond distances and bond orders by Raman spectroscopy. *J. Phys. Chem.* **95,** 5031 (1991).
32. Goodenough, J. B. The two components of the crystallographic transition in VO_2. *J. Solid State Chem.* **3,** 490 (1971).
33. Zylbersztejn, A. & Mott, N. F. Metal-insulator transition in vanadium dioxide. *Phys. Rev. B* **11,** 4383 (1975).
34. Goodenough, J. B. Narrow-band electrons in transition-metal oxides. *Czech. J. Phys. B* **17,** 304 (1967).

Acknowledgements

This work was supported by the U.S. Department of Energy, Office of Science, Basic Energy Sciences, Materials Sciences and Engineering Division. The Raman and high temperature XRD measurements were conducted as a user project at the Centre for Nanophase Materials Sciences (CNMS), which is sponsored at Oak Ridge National Laboratory by the Scientific User Facilities Division, U.S. Department of Energy.

Author Contributions

S.L. conceived and designed the experiments under supervision of H.N.L. S.L. fabricated the samples and measured electrical transport. S.L. also conducted high temperature XRD measurements with help of J.K.K. I.N.I performed Raman spectroscopic measurements. S.L. and H.N.L. wrote the manuscript and other authors reviewed it.

Additional Information

Competing financial interests: The authors declare no competing financial interests.

How to cite this article: Lee, S. *et al.* Epitaxial stabilization and phase instability of VO_2 polymorphs. *Sci. Rep.* **6**, 19621; doi: 10.1038/srep19621 (2016).